Theoretical Investigation on the Mechanism and Law of Broadband Terahertz Wave Detection Using Rydberg Quantum State

Yanchen Zhou , Ruijie Peng, Jinbiao Zhang, Linjie Zhang , Zhenfei Song , Zhigang Feng , and Yan Peng , *Member, IEEE*

Abstract—The bandwidth and sensitivity of traditional terahertz detection devices are limited by material properties and working temperature. Here, we proposed a four-level Rydberg atom detection method, which can realize real-time detection for the absolute strength of the terahertz electric field under room temperature with the detection bandwidth of 0-5 THz. By theoretical analysis and formula derivation, the relation among the terahertz electric field strength, excitation energy level, coupling photoelectric field strength, gas cell temperature and electromagnetically induced transparency (EIT) signal are studied in detailed. The NEP of this method is proven to be 10^{-17} W/Hz$^{1/2}$ in the range of 0-1 THz, which is three orders of magnitude smaller than that of the traditional optimal thermal detection system. This research has important reference value for the later high-sensitivity detection and application development of terahertz waves

Index Terms—NEP, rydberg atom, terahertz wave, terahertz detection.

I. INTRODUCTION

TERAHERTZ waves are the electromagnetic waves with frequencies between 0.1 and 10.0 THz, which is in the transition region between electronics and photonics [1], [2].The low photon energy and strong penetration properties make it have great application potential in non-destructive testing [3], [4]. Therefore, the research of terahertz devices has become a hot topic in the field [5], [6]. In the past forty years, terahertz radiation sources and detectors has made great development.

Yanchen Zhou, Ruijie Peng, Jinbiao Zhang, and Yan Peng are with the Terahertz Technology Innovation Research Institute, Shanghai Key Lab of Modern Optical System and Shanghai Cooperation Innovation Centre of Terahertz Spectroscopy and Imaging Technology, University of Shanghai for Science and Technology, Shanghai 200093, China (e-mail: 13764310515@163.com; 1023240746@qq.com; 809893695@qq.com; py@usst.edu.cn).

Linjie Zhang is with the State Key Lab of Quantum Optics and Quantum Optics Devices, Institute of Laser Spectroscopy, Shanxi University, Taiyuan 030006, China (e-mail: zlj@sxu.edu.cn).

Zhenfei Song and Zhigang Feng are with the Center for Advanced Measurement Science, National Institute of Metrology, Beijing 100029, China (e-mail: songzf@nim.ac.cn; fengzg@nim.ac.cn).

Combing with the coherent detection, more and more detection technologies such as photoconductive antennas [7], electro-optical crystals [8], and air detection [9], [10] have gradually matured. The phase information of the electric field is obtained on the basis of the original detection relative intensity, and the minimum detectable power is also getting smaller and smaller. In addition, the working environment no longer requires ultra-low temperature. Based on the above advantages, coherent detection has become the main detection technology for terahertz waves. However, the obtained terahertz electric field signal is a relative intensity rather than an absolute intensity. At present, one detection method for the absolute intensity of THz wave is the thermal radiation detector, but the device is bulky and the response speed is slow (millisecond level); the other one is the semiconductor material detection method, whose equivalent noise power (NEP) could be at the order of 10^{-12} [11]–[13], and the preparation process is complicated and costly.

This paper proposes to use the Rydberg quantum state detection method to solve the above problems [14]. This technology uses alkali metal atoms as sensors, which can achieve accurate, real-time, high-sensitivity detection at room temperature. Alkali atom refers to the atom with only one electron in its outermost layer, such as Na, Rb and Cs, which is very sensitive to the disturbance of external electric field. When it is used in electro-magnetic field detection, it has sensitive narrow-band response characteristics according to the principle that the incident light energy must be strictly equal to the transition energy level difference. In addition, since each atom of the same isotope has the same properties, detection based on this atomic level can be accurately calibrated to the international system of units (SI). Based on this principle, different frequencies of light can be detected by coupling to quantum states with different energy levels. At present, several research groups have carried out related studies on the application of Rydberg quantum state for accurate detection in microwave band [15]–[20]. This method of measuring electric field has following advantages: 1) The terahertz electric field intensity measurement based on the international unit (Planck constant) standard is produced; [21] 2) because of the invariance of atomic parameters, this method has the ability of self-calibration in terahertz electric field measurement; 3) The medium has almost no loss in the process of terahertz wave detection and transmission; 4) it can measure intense and

weak fields over a wide frequency range; 5) it can be used to build small and portable detectors. Therefore, this method has a broad application prospect for terahertz detector and terahertz biomedical imaging [22], [23].

However, the frequency and photon energy of terahertz wave are higher than those of microwave, so to detect the THz, Rydberg atom needs to be excited to the energy level with lower main quantum number. In addition, the current terahertz beam can be divided into two categories: 1) pulse THz wave, which can cover the entire energy level range of Rydberg atomic transition with the energy level of millivolt [24], [25]. This is far lower than that of the volt level of microwave signal, so the detection device need to be very sensitive, and the requirements for environmental interference control is strict; 2) continuous THz wave, whose energy is higher, but their frequencies are discrete with narrow bandwidth. This lead to the frequency difference between obtainable THz continuous wave and alkali metal atomic energy level is usually more than 100 MHz [26]. Even through the regulation of electric field and magnetic field, it is still difficult to reach this magnitude [27]. Therefore, it is difficult to do the systematic experiment at this stage.

Here, we theoretically studied and derivated the mechanism of broadband THz wave detected by Rydberg quantum state. The relation among the terahertz electric field strength, frequency, excitation energy level, atomic density, gas cell temperature and EIT signal are studied in detailed, and the simulation results are compared with the microwave band. At the end of the paper, the sensitivity limit of the device in the ideal state is deduced. In summary, this paper analyzes an accurate measurement method of broadband terahertz field, which lays a foundation for the subsequent application of this detection technology to the accurate detection of terahertz wave.

II. FUNDAMENTAL PRINCIPLE OF TERAHERTZ ELECTRIC FIELD DETECTION BY RYDBERG ATOM

Rydberg atom [28] is a system of atom in which only one electron be excited into a high quantum state. The electron is so far away from the atomic core (inner electron plus nucleus) that it acts like a point charge. At this time, the atomic system can be considered as a hydrogen-like system, so that the multi-electron atomic system can be transformed into a single-electron atomic system for processing, simplifing the study of the atomic structure, and then the quantum theory of single-electron atomic system can be used to carry out related calculations.

The interaction between Rydberg atom and external electric field causes the Rydberg atom levels to split, which is known as the Aulter-Townes (AT) split. The electromagnetically induced transparency (EIT) [29] effect is a nonlinear quantum coherence effect shown by the interaction between light and matter. In other words, a medium strongly absorbs a light beam at a certain frequency, and when another beam with a different frequency incidents on the medium, the absorbance of the first light beam will be reduced. In the experiment, the AT splitting can be observed through EIT spectrum, and the splitting value is related to the external electric field intensity, Planck constant and transition dipole moment, and then the corresponding external electric field
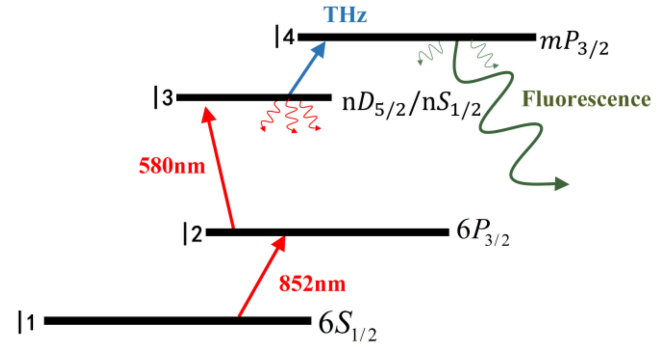

Fig. 1 Schematic diagram of four-level coupling of cesium Rydberg atom.

intensity can be calculated. The high accuracy of this method is determined by the EIT technology [30], which converts the measurement of amplitude to the measurement of frequency. Precise measurements of terahertz electric field can be realized by tuning atoms into different quantum states, each of which corresponds to a specific frequency. Compared with many current methods for electric field measurement, which require complex traceability chain to international unit standard, this measurement technology provides a more direct traceability method.

III. THEORETICAL MODEL

A. A Four-Level System Constructed by Rydberg Quantum State and Applied Electric Field

Simulated medium is a cesium atomic vapor cell with the shape of cube ($20*20*20$ mm^3). The probe laser (852 nm) is locked on the cesium atomic transition level of $6S_{1/2}$—$6P_{3/2}$, the coupling light (580 nm) is scan between $6P_{3/2}$—$nD_{5/2}$ and $6P_{3/2}$—$nS_{1/2}$. The probe laser and the coupling laser propagate in opposite directions and coincide with each other along the axial direction in the cesium vapor cell. As a result, a ladder type three level system is formed, in which the change of probe laser intensity can be obtained from EIT spectrum. The power of probe laser and coupling laser are set as 5 mW and 0.5 W, respectively. Their spot diameter are both 3 mm [31], [32].

When the atomic states nS/nD and mP$_{3/2}$ are selected, the two Rydberg states excited by an external terahertz electric field at a specific frequency are coupled together, forming a four-level system from the original stepped three-level system. This process is shown in Fig. 1. At this time, the energy level |4 is affected by the terahertz Rabi frequency (Ω_{THz}), which results in the interference for the probe laser absorption, and then the EIT peak is divided into two parts, i.e., the AT splitting of the EIT spectrum.

This paper simulates the cesium atom four level Rydberg atomic system, and its free atomic Hamiltonian can be written as:

$$H_A = \frac{p^2}{2m} - \hbar\omega_{01}|1\rangle\langle1|\hbar\omega_{03}|3\rangle\langle3|\hbar\omega_{04}|4\rangle\langle4| \qquad (1)$$

We have taken the state 2 to have zero energy and $\hbar\omega_{01,03,04}$ are energy gaps between four states 1, 3, 4, and state 2. Only the energy in state 1 is negative. In the dipole and rotating-wave

approximations, the atom-field interaction Hamiltonian is:

$$H_{AF} = -\mathbf{d}^{(+)} \cdot \mathbf{E}^{(-)} - \mathbf{d}^{(-)} \cdot \mathbf{E}^{(+)} \tag{2}$$

The dipole operator d has its positive and negative-rotating components. The time-independent Hamiltonian of the system can be obtained by unitary transformation and formula simplification.

$$
\begin{aligned}
H = {} & \frac{p^2}{2m} + \hbar\Delta_1|1\rangle\langle1| + \hbar\Delta_2|3\rangle\langle3| + \hbar\Delta_3|4\rangle\langle4| \\
& + \frac{\hbar}{2}\Omega_1 \left(|1\rangle\langle2|e^{-i\boldsymbol{k_1}\boldsymbol{r}} + |2\rangle\langle1|e^{+i\boldsymbol{k_1}\boldsymbol{r}}\right) \\
& + \frac{\hbar}{2}\Omega_2 \left(|2\rangle\langle3|e^{-i\boldsymbol{k_2}\boldsymbol{r}} + |3\rangle\langle2|e^{+i\boldsymbol{k_2}\boldsymbol{r}}\right) \\
& + \frac{\hbar}{2}\Omega_3 \left(|3\rangle\langle4|e^{-i\boldsymbol{k_3}\boldsymbol{r}} + |4\rangle\langle3|\,e^{+i\boldsymbol{k_3}\boldsymbol{r}}\right)
\end{aligned}
\tag{3}
$$

By substituting the variables into the expression, the evolution of the density matrix is used to describe the system evolution, and each element in the matrix is represented according to the calculation formula of the elements of the density matrix. Finally, by solving the density matrix equations, the susceptibility of the medium for the probe laser, χ, and ς_0 is the dielectric constant under vacuum state. We can give the magnetic susceptibility as [33]:

$$\chi = \frac{jN|\wp_p|\Omega_p}{|E_p|\varsigma_D} \frac{(\Omega_{\text{Thz}})^2 + 4D_{13}D_{14}}{D_{12}(\Omega_{\text{Thz}})^2 + D_{14}(\Omega_c)^2 + 4D_{12}D_{13}D_{14}} \tag{4}$$

$$D_{1i} = \gamma_{1i} - j\Delta_p \tag{5}$$

Among them, N is the atom density in the cell, the characters of the subscript 12, 13 and 14 refer to the transition level 1, 2, 3, and 4, respectively. γ_{1i} represents the attenuation rate at each level [16], Δp is the detuning of the probe laser, $\Omega_{p,c,THz}$ are the Rabi frequencies for the different transitions(probe, coupling, and THz) and are given by:

$$\Omega_{p,c,THz} = |E_{P,c,THz}| \frac{\wp_{P,c,THz}}{\hbar} \tag{6}$$

Here, $\hbar$ is Planck's constant, $E_{p,c,THz}$ are the magnitude of the probe laser field, the coupling laser, and the THz source. $\wp_{p,c,THz}$ are the atomic dipole moments corresponding to the probe, coupling, and RF transitions. Parameters D_{13} and D_{14} [15] would also be a function of Δ_C and Δ_{THz} (the detuning of the coupling laser and THz source), respectively. As the frequencies of coupling laser and terahertz wave are corresponding to the transition energy levels, the terahertz electric field intensity can be directly traced back to the international standard of measurement parameters (the Planck constant), see (6).

Using this magnetization coefficient, the transmission coefficient T of probe light through the atomic vapor cell can be obtained [17]:

$$\left||T| = exp\left(-\frac{2\pi LIm[\chi]}{2\lambda_p}\right)\right| \tag{7}$$

Where L represents the length of the cell and λp is the wavelength of the probe laser. The intensity of the probe laser measured on the detector is given by:

$$I = I_0|T|^2 = I_0 exp\left(-\frac{2\pi LIm[\chi]}{2\lambda_p}\right) \tag{8}$$

I_0 is the intensity of the probe laser at the input of the gas cell. We use this model to understand the behavior of the EIT signal on the detector as a function of the RF field intensity. When the value of $Im[\chi]$ approaches 0, the transmitted signal peak can be observed on the detector. Here, the interval between the two EIT peaks is the AT splitting interval (Δf), and there is a relationship between Δf and the applied electric field Rabi frequency:

$$\Omega_E = 2\pi\Delta f \tag{9}$$

At this time, the electric field intensity of the applied terahertz field can be deduced from the Rabi frequency:

$$|E_E| = \frac{\hbar}{\wp_E}\ \Omega_E = 2\pi\frac{\hbar}{\wp_E}\Delta f \tag{10}$$

B. Calculation of Atomic Transition Dipole Moment

After measuring the splitting interval, an unknown quantity that can determine the electric field intensity is the transition dipole moment of the terahertz transition. The expression of the dipole moment is mentioned in the reference [34] :

$$\wp_E = e\vec{\epsilon}\int \psi_3^*\vec{r}\psi_4^* dV = eA_{34}R_{34} \tag{11}$$

Here e is the elementary charge, $\vec{\epsilon}$ is the polarization vector of light, and Ψ_3^* and Ψ_4^* are the wave functions for the initial and final states of the terahertz field transition. And A_{34} is the angular part and R_{34} is the radial part. Considering the alkali metal atom with a single valence electron, the Hamiltonian of the system can be written as:

$$H = -\frac{1}{2}\nabla^2 + V(r) + Fz \tag{12}$$

After expanding the simplified calculation, the radial matrix elements can be calculated as [35]:

$$E,l\,|r^\sigma|\,E',l' = \sum_i X_i X_i' r_i^{(2+\sigma)} \left(\sum_i X_i^2 r_i^2 \sum_j X_j^2 r_j^2\right)^{-\frac{1}{2}} \tag{13}$$

According to the Eq. (9), we can directly trace the measurement of electric field strength to the international standard physical quantity (Planck constant).

Here, we calculate the atomic transition dipole moment in the terahertz band and compare it with the case of microwave band, as shown in Fig. 2. Here, the main quantum number range of the response energy level in the microwave band and terahertz band are 44–49 [Fig. 2(a)], and 18–23 [Fig. 2(b)], respectively. This is because the frequency of terahertz wave is higher than that of microwave, the photon energy is stronger, and the lower energy level states with larger energy level spacing are needed. The results of Fig. 2 show that the atomic dipole moment decreases with the increase of response frequency, and the atomic dipole moment in terahertz band is one fifth of that in microwave band.
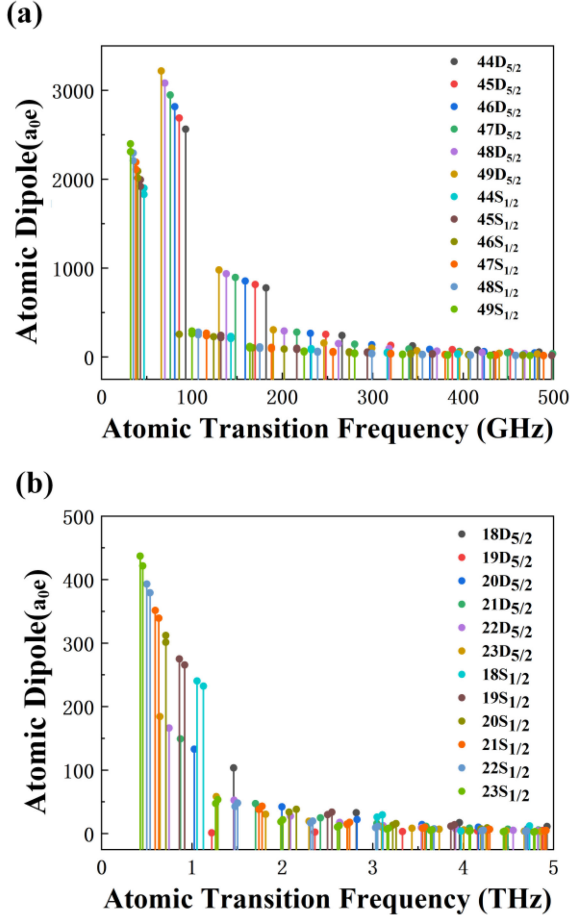
(a)

(b)

Fig. 2. Schematic diagram of coupling response at (a) GHz Band N = 44-49. (b) THz Band N = 18-23.
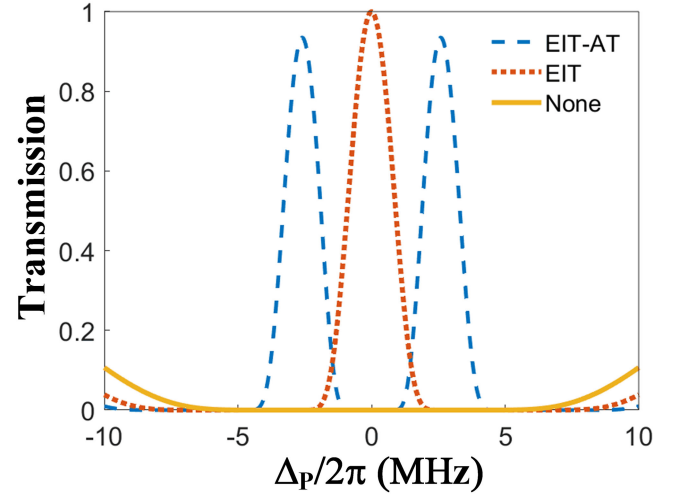

Fig. 3. EIT signal without both coupling laser and terahertz waves (yellow solid line), EIT signal with only coupling laser (red dotted line), EIT-AT signal with both coupling laser and terahertz waves (blue dash line).
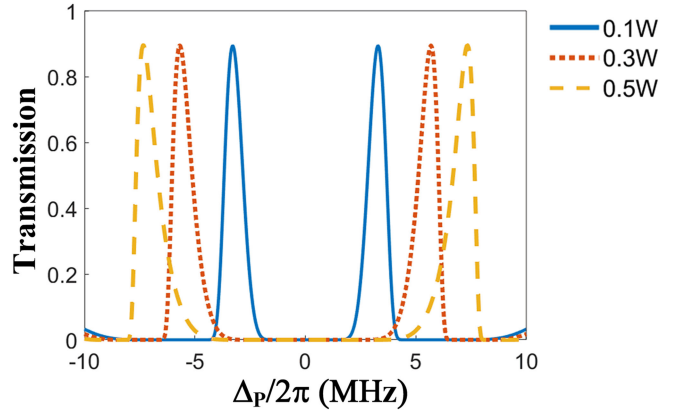

Fig. 4. EIT-AT signal under different applied terahertz electric field strength. The blue solid line, red dotted line and yellow dash line correspond to the intensity of 0.1 W, 0.3 W and 0.5 W, respectively.

C. EIT Response of Terahertz Waves

By adjusting the terahertz waves and coupling laser, the EIT signal and AT splitting phenomenon of cesium Rydberg atom can be observed. As shown in Fig. 3, when only probe laser is applied to the cesium vapor cell, its energy is absorbed by the atomic material. At this moment, there is no EIT signal (the yellow solid line). When the probe laser and the coupling laser act simultaneously, the EIT effect will be generated in the cesium vapor cell and the signal peak will be generated, as the red dotted line shown. When the terahertz field is applied, EIT signal will show AT splitting (the blue dash line).

Due to the influence of Doppler effect, the EIT-AT splitting interval Δf shown in Fig. 3 has the following relation with the Rabi frequency Ω_{THz} of the terahertz electric field coupled with two Rydberg states [36]:

$$\Delta f = \frac{1}{2\pi}\frac{\lambda_c}{\lambda_p}\Omega_{THz} \qquad (14)$$

D. Relationship Between Terahertz EIT and Electric Field Intensity

In order to simulate the interaction between terahertz electric field and cesium atom quickly and simply, the THz electric field in the cell is treated as plane wave here. When the applied

electric field frequency is 1.461 THz, we simulate the corresponding EIT-AT splitting spectrum. As shown in Fig. 4, The splitting degree of EIT-AT signal increases with the increase of the intensity of the applied THz wave. This demonstrates the Rydberg atom's function as a detector of the signal's field strength.

E. Broadband Coverage of Terahertz EIT

The detection method proposed in this paper is suitable for the detection of multiple THz frequencies or broadband THz waves. Here, we enumerated and calculated the Rydberg atomic detection frequency from 0 to 1.5 THz, the corresponding data are presented in Table I. The response frequency of each row in the table is the minimum frequency in the terahertz band that the energy level 3 can be responded. For example, in the first row of the table, the minimum detectable frequency of energy level 3 ($18D_{5/2}$) is 1.461 THz. By comparing the data of each row, it can be found that with the increase of the main quantum number of level 3, the minimum detectable terahertz

TABLE I
RESPONSE FREQUENCY AND ATOMIC DIPOLE MOMENT BETWEEN THE ENERGY LEVEL 3 AND LEVEL 4

| Energy level 3	Energy level 4	Response frequency (THz)	Atomic dipole moment $(a_0 e)$
$18D_{\frac{5}{2}}$	$20p_{\frac{3}{2}}$	1.461	103.426
$19D_{\frac{5}{2}}$	$21p_{\frac{3}{2}}$	1.218	117.738
$20D_{\frac{5}{2}}$	$22p_{\frac{3}{2}}$	1.026	132.978
$21D_{\frac{5}{2}}$	$23p_{\frac{3}{2}}$	0.872	149.146
$22D_{\frac{5}{2}}$	$24p_{\frac{3}{2}}$	0.747	166.241
$23D_{\frac{5}{2}}$	$25p_{\frac{3}{2}}$	0.646	184.264
$18S_{\frac{1}{2}}$	$18p_{\frac{3}{2}}$	1.127	232.273
$19S_{\frac{1}{2}}$	$19p_{\frac{3}{2}}$	0.92	265.677
$20S_{\frac{1}{2}}$	$20p_{\frac{3}{2}}$	0.711	301.320
$21S_{\frac{1}{2}}$	$21p_{\frac{3}{2}}$	0.634	339.203
$22S_{\frac{1}{2}}$	$22p_{\frac{3}{2}}$	0.536	379.324
$23S_{\frac{1}{2}}$	$23p_{\frac{3}{2}}$	0.456	421.685
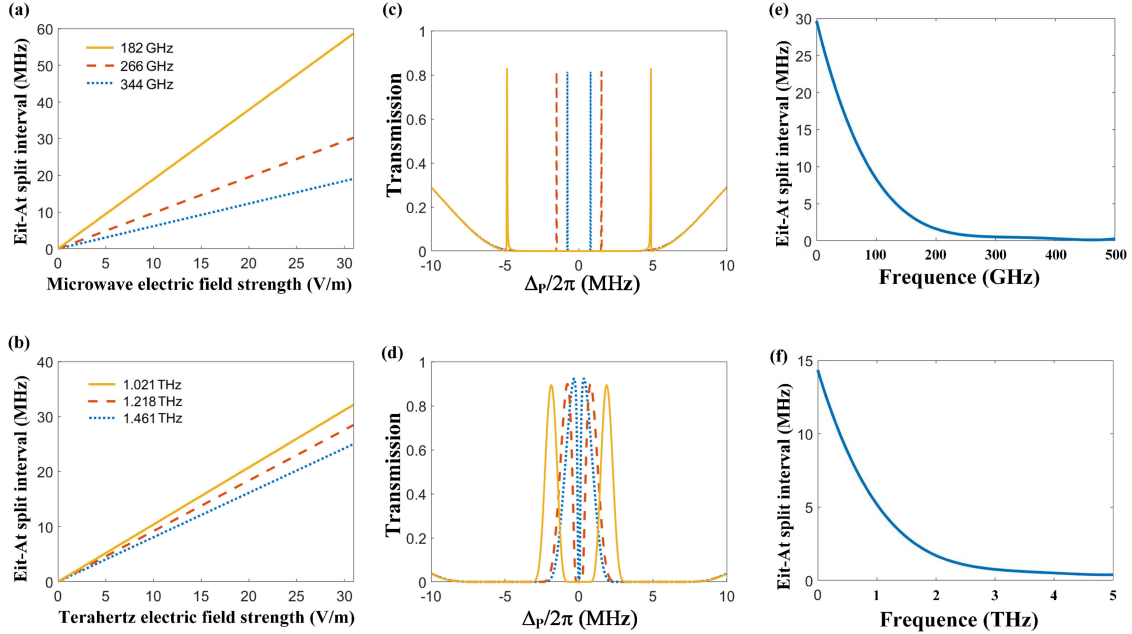
Fig. 5. Under different (a)MW (b)THz electric field frequency, the relation between EIT-AT splitting amplitude and applied electric field intensity. Under the same applied electric field intensity (E = 30 V/m), EIT-AT phenomenon at different (c)MW (d)THz frequencies, and the relation between the EIT-AT split interval and the frequency of the applied (e) MW (f)THz electric field.

frequency will decrease. For the same main quantum number of level 3, the detectable terahertz frequency of the S-Layer is less than that of the D-Layer. We can also conclude that: as the detected terahertz frequency decreases, the atomic dipole moment increases. The coupling efficiency of the device for detecting 0.456 THz is more than three times higher than that for detecting 1.461 THz in Table I, so it can be inferred that the device will be more sensitive for measuring low frequency THz waves.

F. EIT Phenomena at Different THz Frequencies

On the premise of not changing the parameters of the probe&coupling laser, the splitting trend of EIT-AT at different terahertz frequencies is simulated and compared with the case of microwave band, as shown in Fig. 5. Here, the energy level 3 of terahertz and microwave band are chosen as 18 and 44. The EIT-AT splitting amplitude at different frequencies is shown in Fig. 5(a) and (b), Each taking three frequencies as examples,
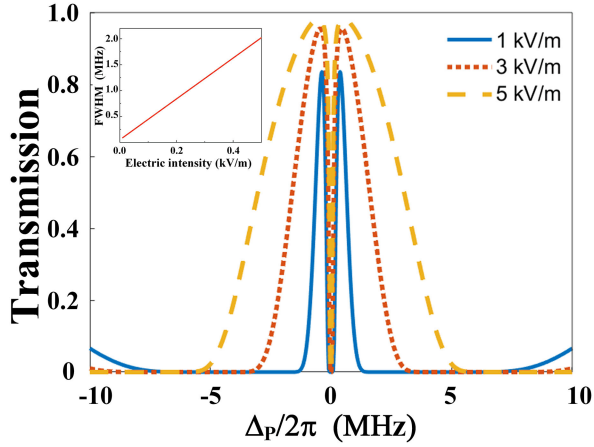
Fig. 6. EIT-AT signal changes under different coupling laser field intensities. We choose 1 kV/m (blue solid line), 3 kV/m (red dot line), 5 kV/m (yellow dash line) as examples. The inset shows the FWHM of EIT-AT splitting peak by as a function of the intensity of coupling laser field.
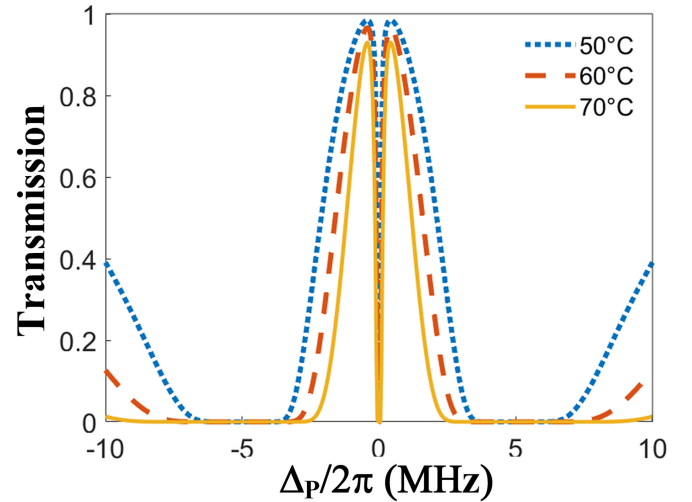

Fig. 7. EIT-AT signal at 1.461 THz, and the temperature of gas cell is 50°C (blue dotted line), 60°C (red dotted line) and 70°C (yellow solid line), respectively.

the EIT-AT splits all show a linear variation, and with the decrease of the applied MW/THz wave frequency, the splits interval becomes larger (represented by the increase of slope in the figure).

According to Eqs. (4) and (9), it can be inferred that the value of coupling optical Rabi frequency in terahertz band is higher than that in microwave band, which leads to the larger full width at half maxima(FWHM) of terahertz EIT signal. In addition, the AT split width in the microwave band is more than two times larger than that in the terahertz band due to the difference of the Rabi frequency in Fig. 5(c) and (d). Therefore, for both THz and MW cases, the EIT detection method is more sensitive to the low frequency fields.

As shown in Fig. 5(e) and (f), we also simulated the variation trend of EIT-AT splitting width at different frequencies without changing the applied MW/THz electric field intensity (30 V/m). Since the atomic dipole moment between the energy levels in the microwave region is much larger than that of the terahertz band, therefore the splitting amplitude of the microwave is twice than that of the terahertz region. Both of them prove that the split size gradually decreases as the frequency increases.

G. Terahertz EIT Phenomena Under Different Coupling Electric Field Intensities

In order to understand the influence of the coupled optical power on the signal of the EIT-AT signal, we fixed $E_{THz} = 0.3$ V/m for simulation in Fig. 6, When the coupling laser power intensity increases from 1 kV/m (blue solid line) to 5 kV/m (yellow dash line), the detuning range of the EIT-AT signal becomes wider. This is because that the intensity change of the coupling laser will directly affect the Rabbi frequency of the coupling laser [(4)]. Obviously, as the coupling electric field intensity is 1 kV/m, the peak value of EIT-AT signal is weaker than others. By comparing the relation between the intensity of the coupled light electric intensity and the FWHM of EIT-AT signal, we can find that there is a linearly proportional

relationship between them, as shown in the inset of the Fig. 6. In addition, we notice that the splitting width of EIT-AT signal does not change with the coupling laser intensity, but its FWHM becomes wider with the increase of the intensity of the coupling laser, which can be used to analyze the intensity of the coupling laser used in the experiment.

H. Terahertz EIT Phenomenon Under Different Coupling Photoelectric Field Intensities

The THz detection technology uses a sealed alkali gas cell as a medium, and its EIT-AT signal is dependent on the atom density. According to (15), It can be found that the atom density is related to temperature [22], [23]:

$$N = \frac{P_V(T) N_A}{RT} \quad (15)$$

N is the atom density of alkali metal atoms in the cell, N_A is Avogadro's constant, and R is the gas constant. The saturated vapor pressure $P_V(T)$ of alkali metal vapor is determined by the temperature T at the interface between alkali metal liquid and vapor. Taking cesium as an example, $P_V(T) = 10^{7.046\text{-}3830/T}$.

In order to study the influence of temperature in the cell on the EIT-AT signal, we simulated the signal at 1.461 THz of different temperatures without changing the applied electric field strength, as shown in Fig. 7. As the temperature of the cesium cell increases from 50°C (blue dot line) to 70°C (yellow solid line), the pressure in the gas cell increases five times [(15)], which result in the increase of detuning range of the probe light, but the FWHM and the intensity of signal will decrease with the increasing temperature. On the other hand, high temperature will increase the instability of atomic reaction. Therefore, in order to get the best detection results, it is necessary to control the chamber temperature reasonably.
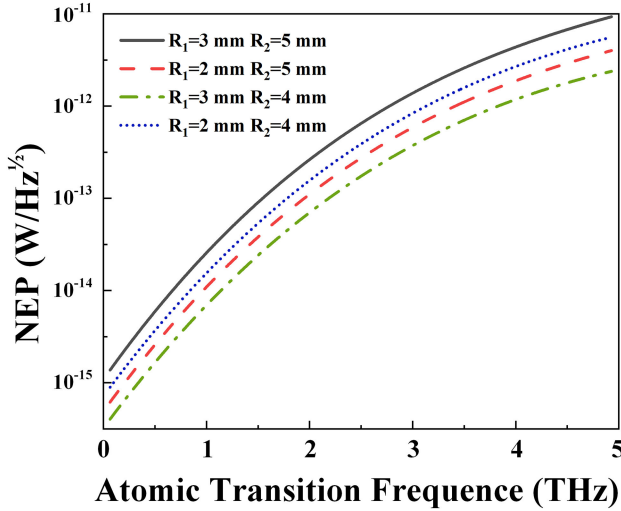
Fig. 8.   Relationship between spot diameter of each beam and NEP.

Fig. 9.   NEP variation rule of Rydberg quantum detection system in response to terahertz waves with different frequencies.

I. The Minimum Detectable Power of the System – NEP

Noise-equivalent power (NEP) [37], [38] represents the sensitivity of photodetector or detector system. For the detection device, it can represent the minimum power that can be measured by the detector [39]:

$$NEP = \frac{P}{SNR} = P \qquad (16)$$

In this paper, the value of the simulated detection bandwidth (*BW*) is 1 Hz, so the formula can be changed as follows:

$$NEP = \frac{P}{\sqrt{BW}} = P \qquad (17)$$

In the free space of electromagnetic radiation, the power flux density (PFD) is the power per unit area perpendicular to the direction of electromagnetic wave propagation, and its unit is W/m^2 [40], represented here by *S*. For the plane wave, power flux density, electric field strength (*E*) and magnetic field intensity (H) and the free space of the inherent impedance: $\eta_0 = 377\ \Omega$.

$$S = \frac{E^2}{\eta_0} = H^2\eta_0 \qquad (18)$$

The equivalent power *P* of a region is the product of PFD and region *A*:

$$P = S \times A \qquad (19)$$

According to Eq. (17), the minimum detectable power of each frequency point is related to the spot diameter of each beam, and the minimum detectable power of the comparison system can be calculated by changing the spot size of each laser beam, and logarithmic processing is carried out on the theoretical calculated value of NEP. As shown in Fig. 8, R_1 is the spot radius of probe laser and coupling laser, and R_2 is the spot radius of terahertz light in millimeters.

As can be seen from Fig. 8, if $R_1 = 3$ mm, we only change the THz beam spot size R_2 from 5 mm (black solid line) to 4 mm (green dot dash line), the NEP value of Rydberg detection
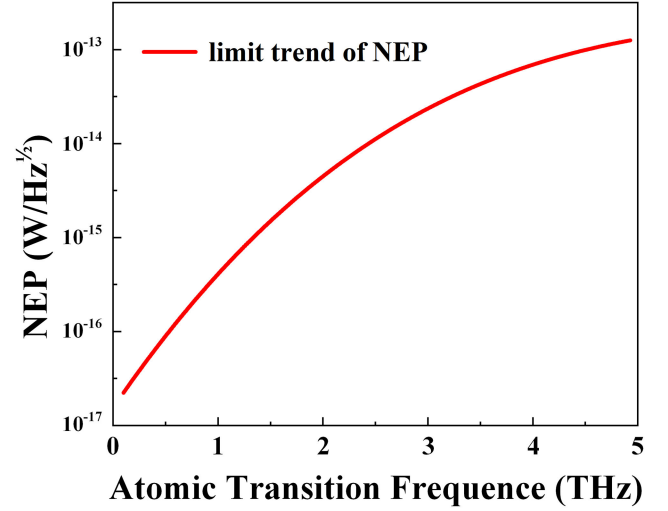
system is generally declining. Similarly, if $R_2 = 5$ mm, the NEP value of the system also shows an overall trend of decline when only the probe and coupling laser spot size R_1 is reduced from 3mm (black solid line) to 2 mm (red dash line). This also means that the smaller the size of each laser spot of the system, the lower the equivalent noise power of the device. Compared with $R_1 = 2$ mm and $R_2 = 5$ mm (red dotted line) and $R_1 = 3$ mm and $R_2 = 4$ mm (green dash line) in the figure, it can be inferred that the NEP value is more affected by the probe and coupling laser spot size than that of the NEP value of $R_1 = 3$ mm and $R_2 = 5$ mm (black solid line).

In order to obtain the minimum detectable power limit of the system, we set the laser spot diameter to 1 mm as an example for simulation. According to the NEP variation rule analysis of the Rydberg quantum detection system as a function of THz waves frequency (Fig. 9), the NEP of the system for low-frequency terahertz light can reach the order of 10^{-17}. The sensitivity of the terahertz electric field detection method based on Rydberg atom is three orders of magnitude higher than that of the most sensitive thermal radiation detector of the present stage, which is only 10^{-14} orders of magnitude.

IV. SUMMARY AND OUTLOOK

In this paper, a detection technique based on Rydberg quantum state to detect the absolute intensity of terahertz wave electric field is analyzed in detail. The variation rule of EIT signal under different parameter conditions (such as applied terahertz electric field intensity, excitation level, coupling photoelectric field intensity and chamber temperature) are summarized. In terms of measurement, the absolute strength of the added signal can be measured directly by conversion, and its equivalent noise power limit can reach 10^{-17} magnitude. These results have important reference value for the development and application of high-sensitivity detection technology in terahertz field.

REFERENCES

[1] G. Liu *et al.*, "Myelin sheath as a dielectric waveguide for signal propagation in the mid-infrared to terahertz spectral range," *Adv. Funct. Mater.*, vol. 29, no. 7, Feb. 2019, Art. no. 1807862.

[2] Y. Peng, C. Shi, Y. Zhu, M. Gu, and S. Zhuang, "Terahertz spectroscopy in biomedical field: A review on signal-to-noise ratio improvement," *Photonix*, vol. 1, no. 1, Apr. 2020, Art. no. 12.

[3] Y. H. Tao, A. J. Fitzgerald, and V. P. Wallace, "Non-contact, nondestructive testing in various industrial sectors with terahertz technology," *Sensors*, vol. 20, no. 3, Feb. 2020, Art. no. 712.

[4] L. Afsah-Hejri, P. Hajeb, P. Ara, and R. J. Ehsani, "A comprehensive review on food applications of terahertz spectroscopy and imaging," *Comprehensive Rev. Food Sci. Food Saf.*, vol. 18, no. 5, pp. 1563–1621, Sep. 2019.

[5] Y. Yang, M. Mandehgar, and D. R. Grischkowsky, "Understanding THz pulse propagation in the atmosphere," *IEEE Trans. Terahertz Sci. Technol.*, vol. 2, no. 4, pp. 406–415, Jul. 2012.

[6] S.-R. Moon, M. Sung, J. K. Lee, and S.-H. Cho, "Cost-effective photonics-based THz wireless transmission using PAM-N signals in the 0.3 THz band," *J. Lightw. Technol.*, vol. 39, no. 2, pp. 357–362, Jan. 2021.

[7] P. A. Obraztsov *et al.*, "Hybrid perovskite terahertz photoconductive antenna," *Nanomaterials*, vol. 11, no. 2, Jan. 2021, Art. no. 313.

[8] J. E. Nkeck, X. Ropagnol, R. Nechache, and F. Blanchard, "Electro-optical detection of terahertz radiation in a zinc sulphide crystal at a wavelength of 512 nm," *Appl. Phys. Exp.*, vol. 13, no. 11, Nov. 2020, Art. no. 112007.

[9] H. W. Du, "Investigation on response function of terahertz air coherent detection technique," *Appl. Phys. B-Lasers Opt.*, vol. 126, no. 7, Jun. 2020, Art. no. 124.

[10] Y. Peng *et al.*, "Experimental measurement of the wake field in a plasma filament created by a single-color ultrafast laser pulse," *Phys. Rev. E*, vol. 102, no. 6, Dec. 2020, Art. no. 063211.

[11] A. Jakhar, V. Dhyani, and S. Das, "Room temperature terahertz detector based on single silicon nanowire junctionless transistor with high detectivity," *Semicond. Sci. Technol.*, vol. 35, no. 12, Dec. 2020, Art. no. 125020.

[12] Z. P. Li *et al.*, "On-chip dual-comb source based on terahertz quantum cascade lasers under microwave double injection," *Phys. Rev. Appl.*, vol. 12, no. 4, Oct. 2019, Art. no. 044068.

[13] M. Jeannin *et al.*, "High temperature metamaterial terahertz quantum detector," *Appl. Phys. Lett.*, vol. 117, no. 25, Dec. 2020, Art. no. 251102.

[14] C. T. Fancher, D. R. Scherer, M. C. S. John, and B. L. S. Marlow, "Rydberg atom electric field sensors for communications and sensing," *IEEE Trans. Quantum Eng.*, vol. 2, 2021, Art. no. 3501313.

[15] C. L. Holloway *et al.*, "Broadband Rydberg atom-based electric-field probe for SI-traceable, self-calibrated measurements," *IEEE Trans. Antennas Propag.*, vol. 62, no. 12, pp. 6169–6182, Dec. 2014.

[16] J. A. Sedlacek, A. Schwettmann, H. Kuebler, R. Loew, T. Pfau, and J. P. Shaffer, "Microwave electrometry with Rydberg atoms in a vapour cell using bright atomic resonances," *Nature Phys.*, vol. 8, no. 11, pp. 819–824, Nov. 2012.

[17] C. L. Holloway *et al.*, "Sub-wavelength imaging and field mapping via electromagnetically induced transparency and Autler-Townes splitting in Rydberg atoms," *Appl. Phys. Lett.*, vol. 104, no. 24, Jun. 2014, Art. no. 244102.

[18] J. A. Gordon *et al.*, "Millimeter wave detection via Autler-Townes splitting in rubidium Rydberg atoms," *Appl. Phys. Lett.*, vol. 105, no. 2, Jul. 2014, Art. no. 024104.

[19] J. A. Sedlacek, A. Schwettmann, H. Kuebler, and J. P. Shaffer, "Atom-based vector microwave electrometry using rubidium Rydberg atoms in a vapor cell," *Phys. Rev. Lett.*, vol. 111, no. 6, Aug. 2013, Art. no. 063001.

[20] C. L. Holloway *et al.*, "Atom-based RF electric field metrology: From self-calibrated measurements to subwavelength and near-field imaging," *IEEE Trans. Electromagn. Compat.*, vol. 59, no. 2, pp. 717–728, Apr. 2017.

[21] D. A. Anderson, R. E. Sapiro, and G. Raithel, "A self-calibrated SI-traceable Rydberg atom-based radio frequency electric field probe and measurement instrument," *IEEE Trans. Antennas Propag.*, vol. 69, no. 9, pp. 5931–5941, Sep. 2021.

[22] S. Ravets, H. Labuhn, D. Barredo, L. Beguin, T. Lahaye, and A. Browaeys, "Coherent dipole-dipole coupling between two single Rydberg atoms at an electrically-tuned forster resonance," *Nature Phys.*, vol. 10, no. 12, pp. 914–917, Dec. 2014.

[23] M. T. Simons, J. A. Gordon, and C. L. Holloway, "Fiber-coupled vapor cell for a portable Rydberg atom-based radio frequency electric field sensor," *Appl. Opt.*, vol. 57, no. 22, pp. 6456–6460, Aug. 2018.

[24] D. M. Mittleman, "Twenty years of terahertz imaging invited," *Opt. Exp.*, vol. 26, no. 8, pp. 9417–9431, Apr. 2018.

[25] Y. Liu, K. Wu, C. Liu, G. Cui, C. Chang, and G. Liu, "Amplification of terahertz/infrared field at the nodes of Ranvier for myelinated nerve," *Sci. China-Phys. Mechanics Astron.*, vol. 63, no. 7, May 2020, Art. no. 274211.

[26] Z. Xiang, C. Tang, C. Chang, and G. Liu, "A primary model of THz and far-infrared signal generation and conduction in neuron systems based on the hypothesis of the ordered phase of water molecules on the neuron surface I: Signal characteristics," *Sci. Bull.*, vol. 65, no. 4, pp. 308–317, Feb. 2020.

[27] L. J. Zhang *et al.*, "Interplay between optical pumping and Rydberg EIT in magnetic fields," *Opt. Exp.*, vol. 26, no. 23, pp. 29931–29944, Nov. 2018.

[28] D. A. Anderson, S. A. Miller, G. Raithel, J. A. Gordon, M. L. Butler, and C. L. Holloway, "Optical measurements of strong microwave fields with Rydberg atoms in a vapor cell," *Phys. Rev. Appl.*, vol. 5, no. 3, Mar. 2016, Art. no. 034003.

[29] A. K. Robinson, A. B. Artusio-Glimpse, M. T. Simons, and C. L. Holloway, "Atomic spectra in a six-level scheme for electromagnetically induced transparency and Autler-Townes splitting in Rydberg atoms," *Phys. Rev. A*, vol. 103, no. 2, Feb. 2021, Art. no. 023704.

[30] C. Carr, M. Tanasittikosol, A. Sargsyan, D. Sarkisyan, C. S. Adams, and K. J. Weatherill, "Three-photon electromagnetically induced transparency using Rydberg states," *Opt. Lett.*, vol. 37, no. 18, pp. 3858–3860, Sep. 2012.

[31] H. Fan, S. Kumar, J. Sheng, J. P. Shaffer, C. L. Holloway, and J. A. Gordon, "Effect of vapor-cell geometry on Rydberg-atom-based measurements of radio-frequency electric fields," *Phys. Rev. Appl.*, vol. 4, no. 4, Oct. 2015, Art. no. 044015.

[32] L. Zhang, J. Liu, Y. Jia, H. Zhang, Z. Song, and S. Jia, "Vapor cell geometry effect on Rydberg atom-based microwave electric field measurement," *Chin. Phys. B*, vol. 27, no. 3, Mar. 2018, Art. no. 033201.

[33] S. N. Sandhya and K. K. Sharma, "Atomic coherence effects in four-level systems: Doppler-free absorption within an electromagnetically-induced-transparency window," *Phys. Rev. A*, vol. 55, no. 3, pp. 2155–2158, Mar. 1997.

[34] I. I. Sobelman, *Atomic Spectra and Radiative Transitions*. Berlin/ Heidelberg, Germany: Springer, 1979.

[35] C. G. Wade, N. Sibalic, N. R. de Melo, J. M. Kondo, C. S. Adams, and K. J. Weatherill, "Real-time near-field terahertz imaging with atomic optical fluorescence," *Nature Photon.*, vol. 11, no. 1, pp. 40–43, Jan. 2017.

[36] H.-C. Li, G.-Q. Ge, and M. S. Zubairy, "Efficient nonlinear frequency mixing using Autler-Townes splitting," *Phys. Rev. A*, vol. 102, no. 5, Nov. 2020, Art. no. 053701.

[37] R. M. J. Janssen, A. Endo, P. J. de Visser, T. M. Klapwijk, and J. J. A. Baselmans, "Equivalence of optical and electrical noise equivalent power of hybrid NbTiN-Al microwave kinetic inductance detectors," *Appl. Phys. Lett.*, vol. 105, no. 19, Nov. 2014, Art. no. 193504.

[38] R. F. Su *et al.*, "Noise equivalent power of a NbTiN-Al-based kinetic inductance detector for terahertz sensing," *Supercond. Sci. Technol.*, vol. 35, no. 5, May 2022, Art. no. 055016.

[39] H. Fan, S. Kumar, J. Sedlacek, H. Kuebler, S. Karimkashi, and J. P. Shaffer, "Atom based RF electric field sensing," *J. Phys. B-At. Mol. Opt. Phys.*, vol. 48, no. 20, Oct. 2015, Art. no. 202001.

[40] R. L. Pedersen, L. Hogstedt, A. Barh, L. Meng, and P. Tidemand-Lichtenberg, "Characterization of the NEP of mid-infrared upconversion detectors," *IEEE Photon. Technol. Lett.*, vol. 31, no. 9, pp. 681–684, May 2019.